EUROPEAN ORGANISATION FOR NUCLEAR RESEARCH

CERN-PPE/90-95
July 2, 1990

A Direct Search for Neutralino Production at LEP

The OPAL Collaboration

Abstract

A search has been performed for the production of neutralinos (χ, χ') in e^+e^- annihilation at energies near the Z^0 pole. No evidence for these particles was found either in searches for events with two acoplanar jets, low visible energy, and missing p_t (sensitive to $Z^0 \to \chi\chi' \to \chi\chi f\bar{f}$) or in searches for single-photon events (sensitive to $Z^0 \to \chi\chi' \to \chi\chi\gamma$). Model independent upper limits (at the 95% C. L.) on the branching ratio for the decay mode $Z^0 \to \chi\chi'$ of a few 10^{-4} are obtained for most of the range of neutralino masses that is kinematically accessible at LEP energies. Upper limits on the mixing factor of neutralinos are also placed as a function of the neutralino masses.

(Submitted to Physics Letters B)

The OPAL Collaboration

M.Z. Akrawy[11], G. Alexander[21], J. Allison[14], P.P. Allport[5], K.J. Anderson[8], J.C. Armitage[6], G.T.J. Arnison[18], P. Ashton[14], G. Azuelos[16,f], J.T.M. Baines[14], A.H. Ball[15], J. Banks[14], G.J. Barker[11], R.J. Barlow[14], J.R. Batley[5], J. Becker[9], T. Behnke[7], K.W. Bell[18], G. Bella[21], S. Bethke[10], O. Biebel[3], U. Binder[9], I.J. Bloodworth[1], P. Bock[10], H. Breuker[7], R.M. Brown[18], R. Brun[7], A. Buijs[7], H.J. Burckhart[7], P. Capiluppi[2], R.K. Carnegie[6], A.A. Carter[11], J.R. Carter[5], C.Y. Chang[15], D.G. Charlton[7], J.T.M. Chrin[14], P.E.L. Clarke[23], I. Cohen[21], W.J. Collins[5], J.E. Conboy[13], M. Couch[1], M. Coupland[12], M. Cuffiani[2], S. Dado[20], G.M. Dallavalle[2], P. Debu[19], M.M. Deninno[2], A. Dieckmann[10], M. Dittmar[4], M.S. Dixit[17], E. Duchovni[24], I.P. Duerdoth[7,d], D.J.P. Dumas[6], H. El Mamouni[16], P.A. Elcombe[5], P.G. Estabrooks[6], E. Etzion[21], F. Fabbri[2], P. Farthouat[19], H.M. Fischer[3], D.G. Fong[15], M.T. French[18], C. Fukunaga[22], A. Gaidot[19], O. Ganel[24], J.W. Gary[10], J. Gascon[16], N.I. Geddes[18], C.N.P. Gee[18], C. Geich-Gimbel[3], S.W. Gensler[8], F.X. Gentit[19], G. Giacomelli[2], V. Gibson[5], W.R. Gibson[11], J.D. Gillies[18], J. Goldberg[20], M.J. Goodrick[5], W. Gorn[4], D. Granite[20], E. Gross[24], J. Grunhaus[21], H. Hagedorn[9], J. Hagemann[7], M. Hansroul[7], C.K. Hargrove[17], I. Harrus[20], J. Hart[5], P.M. Hattersley[1], M. Hauschild[7], C.M. Hawkes[7], E. Heflin[4], R.J. Hemingway[6], R.D. Heuer[7], J.C. Hill[5], S.J. Hillier[1], C. Ho[4], J.D. Hobbs[8], P.R. Hobson[23], D. Hochman[24], B. Holl[7], R.J. Homer[1], S.R. Hou[15], C.P. Howarth[13], R.E. Hughes-Jones[14], R. Humbert[9], P. Igo-Kemenes[10], H. Ihssen[10], D.C. Imrie[23], A. Jawahery[15], P.W. Jeffreys[18], H. Jeremie[16], M. Jimack[7], M. Jobes[1], R.W.L. Jones[11], P. Jovanovic[1], D. Karlen[6], K. Kawagoe[22], T. Kawamoto[22], R.G. Kellogg[15], B.W. Kennedy[13], C. Kleinwort[7], D.E. Klem[17], G. Knop[3], T. Kobayashi[22], T.P. Kokott[3], L. Köpke[7], R. Kowalewski[6], H. Kreutzmann[3], J. Kroll[8], M. Kuwano[22], P. Kyberd[11], G.D. Lafferty[14], F. Lamarche[16], W.J. Larson[4], J.G. Layter[4], P. Le Du[19], P. Leblanc[16], A.M. Lee[15], M.H. Lehto[13], D. Lellouch[7], P. Lennert[10], L. Lessard[16], L. Levinson[24], S.L. Lloyd[11], F.K. Loebinger[14], J.M. Lorah[15], B. Lorazo[16], M.J. Losty[17], J. Ludwig[9], J. Ma[4,b], A.A. Macbeth[14], M. Mannelli[7], S. Marcellini[2], G. Maringer[3], A.J. Martin[11], J.P. Martin[16], T. Mashimo[22], P. Mättig[7], U. Maur[3], T.J. McMahon[1], J.R. McNutt[13], A.C. McPherson[6,c], F. Meijers[7], D. Menszner[10], F.S. Merritt[8], H. Mes[17], A. Michelini[7], R.P. Middleton[18], G. Mikenberg[24], D.J. Miller[13], C. Milstene[21], M. Minowa[22], W. Mohr[9], A. Montanari[2], T. Mori[22], M.W. Moss[14], P.G. Murphy[14], W.J. Murray[5], B. Nellen[3], H.H. Nguyen[8], M. Nozaki[22], A.J.P. O'Dowd[14], S.W. O'Neale[7,e], B.P. O'Neill[4], F.G. Oakham[17], F. Odorici[2], M. Ogg[6], H. Oh[4], M.J. Oreglia[8], S. Orito[22], J.P. Pansart[19], G.N. Patrick[18], S.J. Pawley[14], P. Pfister[9], J.E. Pilcher[8], J.L. Pinfold[24], D.E. Plane[7], B. Poli[2], A. Pouladdej[6], T.W. Pritchard[11], G. Quast[7], J. Raab[7], M.W. Redmond[8], D.L. Rees[1], M. Regimbald[16], K. Riles[4], C.M. Roach[5], S.A. Robins[11], A. Rollnik[3], J.M. Roney[8], S. Rossberg[9], A.M. Rossi[2,a], P. Routenburg[6], K. Runge[9], O. Runolfsson[7], S. Sanghera[6], R.A. Sansum[18], M. Sasaki[22], B.J. Saunders[18], A.D. Schaile[9], O. Schaile[9], W. Schappert[6], P. Scharff-Hansen[7], S. Schreiber[3], J. Schwarz[9], A. Shapira[24], B.C. Shen[4], P. Sherwood[13], A. Simon[3], P. Singh[11], G.P. Siroli[2], A. Skuja[15], A.M. Smith[7], T.J. Smith[1], G.A. Snow[15], R.W. Springer[15], M. Sproston[18], K. Stephens[14], H.E. Stier[9], R. Stroehmer[10], D. Strom[8], H. Takeda[22], T. Takeshita[22], T. Tsukamoto[22], M.F. Turner[5], G. Tysarczyk-Niemeyer[10], D. Van den plas[16], G.J. VanDalen[4], G. Vasseur[19], C.J. Virtue[17], H. von der Schmitt[10], J. von Krogh[10], A. Wagner[10], C. Wahl[9], C.P. Ward[5], D.R. Ward[5], J. Waterhouse[6], P.M. Watkins[1], A.T. Watson[1], N.K. Watson[1], M. Weber[10], S. Weisz[7], P.S. Wells[7], N. Wermes[10], M. Weymann[7], G.W. Wilson[19], J.A. Wilson[1], I. Wingerter[7], V-H. Winterer[9], N.C. Wood[13], S. Wotton[7], B. Wuensch[3], T.R. Wyatt[14], R. Yaari[24], Y. Yang[4,b], G. Yekutieli[24], T. Yoshida[22], W. Zeuner[7], G.T. Zorn[15].

[1]School of Physics and Space Research, University of Birmingham, Birmingham, B15 2TT, UK
[2]Dipartimento di Fisica dell' Università di Bologna and INFN, Bologna, 40126, Italy

[3]Physikalisches Institut, Universität Bonn, D-5300 Bonn 1, FRG
[4]Department of Physics, University of California, Riverside, CA 92521 USA
[5]Cavendish Laboratory, Cambridge, CB3 0HE, UK
[6]Carleton University, Dept of Physics, Colonel By Drive, Ottawa, Ontario K1S 5B6, Canada
[7]CERN, European Organisation for Particle Physics, 1211 Geneva 23, Switzerland
[8]Enrico Fermi Institute and Department of Physics, University of Chicago, Chicago Illinois 60637, USA
[9]Fakultät für Physik, Albert Ludwigs Universität, D-7800 Freiburg, FRG
[10]Physikalisches Institut, Universität Heidelberg, Heidelberg, FRG
[11]Queen Mary and Westfield College, University of London, London, E1 4NS, UK
[12]Birkbeck College, London, WC1E 7HV, UK
[13]University College London, London, WC1E 6BT, UK
[14]Department of Physics, Schuster Laboratory, The University, Manchester, M13 9PL, UK
[15]Department of Physics and Astronomy, University of Maryland, College Park, Maryland 20742, USA
[16]Laboratoire de Physique Nucléaire, Université de Montréal, Montréal, Quebec, H3C 3J7, Canada
[17]National Research Council of Canada, Herzberg Institute of Astrophysics, Ottawa, Ontario K1A 0R6, Canada
[18]Rutherford Appleton Laboratory, Chilton, Didcot, Oxfordshire, OX11 0QX, UK
[19]DPhPE, CEN Saclay, F-91191 Gif-sur-Yvette, France
[20]Department of Physics, Technion-Israel Institute of Technology, Haifa 32000, Israel
[21]Department of Physics and Astronomy, Tel Aviv University, Tel Aviv 69978, Israel
[22]International Centre for Elementary Particle Physics and Dept of Physics, University of Tokyo, Tokyo 113, and Kobe University, Kobe 657, Japan
[23]Brunel University, Uxbridge, Middlesex, UB8 3PH UK
[24]Nuclear Physics Department, Weizmann Institute of Science, Rehovot, 76100, Israel

[a]Present address: Dipartimento di Fisica, Università della Calabria, 87036 Rende, Italy
[b]On leave from Harbin Institute of Technology, Harbin, China
[c]Now at Applied Silicon Inc
[d]On leave from Manchester University
[e]On leave from Birmingham University
[f]and TRIUMF, Vancouver, Canada

Introduction

In supersymmetric theories[1], the super-partners of the γ, Z^0 and Higgs bosons mix to form four mass eigenstates that are called neutralinos [2,3,4]. Since the Z^0 is expected to have a sizeable coupling strength to a pair of neutralinos, the LEP e^+e^- collider at CERN provides an excellent opportunity to search for neutralinos produced in Z^0 decay.

In this analysis, we assume that the lightest neutralino (χ) is the lightest supersymmetric particle. The heavier neutralinos (χ') can decay into the χ through

$$\chi' \to \chi f \bar{f}$$

$$\chi' \to \chi\gamma.$$

We assume that these are the only decay modes of the χ', and that the masses of the h^0 (Higgs) and $\chi^\pm$ (chargino) are sufficiently large so that $\chi' \to \chi h^0$ and $\chi' \to \chi^\pm f \bar{f}'$ are kinematically forbidden. If R-parity is conserved, the χ is stable; and if the super-partners of the quarks and leptons are heavy, the χ has an interaction cross-section in matter comparable to that of weak interactions. The χ will therefore not be directly observed in the detector.

The aim of this study is a direct search for the production of $\chi\chi'$ pairs. The relevant processes are $e^+e^- \to \chi\chi' \to \chi\chi f\bar{f}$ and $e^+e^- \to \chi\chi' \to \chi\chi\gamma$. In calculating decays, we assume that χ' decays into $\chi f\bar{f}$ are mediated by only the Z^0, which is expected if the mass of the Higgs and the scalar leptons and scalar quarks are assumed to be heavy ($\geq$ 100 GeV/c^2). In this paper, upper limits on the branching ratios $BR(Z^0 \to \chi\chi' \to \chi\chi f\bar{f})$ and $BR(Z^0 \to \chi\chi' \to \chi\chi\gamma)$ are presented as a function of the masses M_χ and $M_{\chi'}$. These results are combined to give an upper limit on the branching ratio $BR(Z^0 \to \chi\chi')$ that is independent of any assumption about the relative strengths of the $\chi' \to \chi f\bar{f}$ and $\chi' \to \chi\gamma$ decays. The limits on these branching ratios are interpreted in the context of the minimal supersymmetric standard model[5], and limits are placed on the mixing factor of the neutralinos.

Apparatus

The data were recorded with the OPAL detector during the 1989 and 1990 LEP runs (through May 1990) during scans of the Z^0 resonance. The center of mass energies ranged from 88.3 to 95.0 GeV. These data correspond to an integrated luminosity of 2.1 pb^{-1}. The OPAL detector is a multipurpose apparatus consisting of a system of central tracking chambers inside a solenoid that provides a uniform magnetic field of 0.436 T. The most important tracking element for this analysis is a cylindrical drift chamber, four meters in length and two meters in radius, containing 159 layers of sense wires in 24 azimuthal sectors. The solenoid is surrounded by time-of-flight scintillation-counters, and a lead-glass electromagnetic calorimeter. Similar calorimetry covers the two endcaps of the detector. The electromagnetic calorimeter consists of a cylindrical array of 9,440 lead-glass blocks, each 10 cm $\times$ 10 cm in cross-section with 24.6 radiation lengths thickness, oriented to point approximately towards the interaction point, and two endcaps of 1,132 lead glass blocks each, with 20.0 radiation lengths thickness, oriented parallel to the beam direction. The iron return yoke of the magnet is instrumented with 9 layers of streamer tubes, which provide hadron calorimetry and muon identification over nearly the whole solid angle. Signals of the hadron calorimeter are read from pads and strips in each layer. Muons are also identified in four layers of drift chambers surrounding the hadron calorimeter. A small-angle calorimeter and proportional tube chambers,

called the forward detector, serves as a luminosity monitor. The components of the OPAL detector are described in more detail elsewhere.[6]

Analysis

The $\chi\chi' \to \chi\chi f\bar{f}$ mode

The cleanest signature of this process is an event topology of large missing momentum and large acoplanarity due to the two undetected neutralinos (χ); hence we searched for acoplanar two-jet events with small visible energy. Jets were defined using the JADE algorithm[9]; since a jet could consist of a single charged particle, lepton-pair events were classified as two-jet events in this analysis. Thus quarks and leptons were treated inclusively for the final state fermion pair.

For the calculation of the quantities used in the following selection, both charged tracks and electromagnetic clusters were used. Tracks were required to satisfy the following conditions:

- The impact parameter (d_0) in the plane transverse to the beam was required to be less than 1 cm,
- the magnitude of z_0, the z coordinate of the point of closest approach to the beam, was required to be less than 35 cm, and
- the number of hits associated to the track was required to be 50 or more.

The energy of each electromagnetic cluster was required to be larger than 100 MeV in the barrel region and 200 MeV in the endcap region. To avoid the double counting of particle energy, clusters in the electromagnetic calorimeter with an associated charged track were eliminated, provided their energy was less than 1.5 GeV, or the ratio between the energy of the cluster and the momentum of the associated track was greater than 0.7 but less than 1.5. If an electromagnetic cluster did not satisfy these conditions, then the cluster was retained and included in the energy and momentum calculations described below.

The visible energy ($E_{\rm vis}$) was defined as the sum of the energy of charged tracks (assuming zero mass) and neutral clusters. Figure 1(a) comparess the distributions of a sample of $\tau\tau$ events (dots) and KORALZ[7] Monte Carlo events (histogram). The distributions of a sample of multihadronic events (dots) and LUND[8] Monte Carlo events (histogram) are shown in Figure 1(b). Satisfactory agreement of the visible energy distributions between the real events and the Monte Carlo events is obtained for both the $\tau\tau$ events and the multihadronic events.

The following cuts were applied to select the events in the data:

(1) The energy deposited in the forward detectors had to be less than 5 GeV.

(2) $|\cos\theta_T| \leq 0.7$, where θ_T is the angle between the thrust axis of the event and the beam direction.

(3) $|z_{\rm vtx}| \leq 10$ cm, where $z_{\rm vtx}$ is the average z_0 of the charged tracks selected by the criteria of the d_0 and the number of hits described above.

Cuts (1)–(3) strongly rejected the backgrounds from beam-wall and beam-gas events.

(4) $E_{\rm vis} \leq E_{\rm beam}$, where $E_{\rm beam}$ is the beam energy.

This cut rejected multihadronic background, Bhabha and $\mu\mu$ events. Figure 2(a) shows the observed visible energy distribution. The peak in the data at low $E_{\rm vis}$ comes from two-photon events.

The following selection criteria were required to select two-jet events.

(5) A jet analysis was performed using the JADE method[9] with the parameter $Y_{\rm min}$ of 0.035. The number of "jets" was required to be equal to two.

(6) At least 1 charged particle with momentum larger than 1 GeV/c was required in each jet.

(7) $|\cos\theta_{jet,i}| \leq 0.8$ (i=1,2),
where $\theta_{jet,i}$ is the angle between the direction of the sum of the momenta in the i-th jet ($\vec{p}_{jet,i}$) and the beam direction.

(8) $\Delta\phi \geq 25°$, where the acoplanarity $\Delta\phi$ is defined by

$$\cos(\Delta\phi) = -\frac{(\vec{p}_{jet,1} \times \vec{p}_e) \cdot (\vec{p}_{jet,2} \times \vec{p}_e)}{|\vec{p}_{jet,1} \times \vec{p}_e| \cdot |\vec{p}_{jet,2} \times \vec{p}_e|},$$

and $\vec{p}_e$ is the momentum of the incoming electron.

Figure 2(b) shows the observed acoplanarity angle distribution after cuts 1–7. The $\chi\chi f\bar{f}$ events tend to have large acoplanarity angles due to the large missing momentum carried by the two undetected neutralinos. This cut eliminates the backgrounds from the $e^+e^- \rightarrow \tau\tau$ process and reduces two-photon backgrounds.

In $\chi\chi f\bar{f}$ events, the vector sum of the transverse momenta in the event ($P_{\rm T,sum}$) may be large due to the undetected neutralinos. Two-photon events without energy deposited in the forward detector tend to have small $P_{\rm T,sum}$. Since the forward detector covers the region $\theta \geq 50$ mrad, the largest $P_{\rm T}$ which can be carried away by an unobserved electron or photon is about 2 GeV/c. To eliminate two-photon background, the following cut was applied:

(9) $P_{\rm T,sum} \geq 5$ GeV/c.

No events survived these cuts. Figure 2(c) shows the event $P_{\rm T,sum}$ distribution after the cuts (1) through (8) (solid histogram).

In order to estimate the significance of this null result, a Monte Carlo simulation of this process was performed. The four-particle final state ($\chi\chi f\bar{f}$) was generated according to the following matrix element [2];

$$\begin{aligned} &d\sigma(e^+(p_1)e^-(p_2) \rightarrow \chi(k_1)\chi'(q_2) \rightarrow \chi(k_1)\chi(k_2)f(p_3)\bar{f}(p_4)) \\ &\quad \propto [(p_3+p_4)^2 - M_Z^2]^{-2}(p_1\cdot k_1 p_2\cdot q_2 + p_1\cdot q_2 p_2\cdot k_1 - \eta\eta' p_1\cdot p_2 M_\chi M_{\chi'}) \\ &\quad \times(p_3\cdot k_2 q_2\cdot p_4 + p_3\cdot q_2 p_4\cdot k_2 + \eta\eta' p_3\cdot p_4 M_\chi M_{\chi'})d\Phi^{(4)}, \end{aligned}$$

where $p_1, p_2, q_2, k_1, k_2, p_3, p_4$ are the 4-momenta of the particles. $M_{\rm Z}$ is the mass of the Z^0 and $d\Phi^{(4)}$ is the four-body phase space; η and η' are the signs in the Majorana condition on χ and χ', respectively ($\eta\eta' = \pm 1$)[4]. The partial decay width of χ' into a particular fermion species is given by [2]

$$\Gamma(\chi' \rightarrow \chi f\bar{f}) \propto [(T_3 - Q\sin^2\theta_W)^2 + Q^2\sin^4\theta_W],$$

where T_3, Q and θ_W are the third component of the weak isospin of the fermion, the electric charge of the fermion and the weak mixing angle, respectively. We have used our measured value of M_Z given in [10] (91.1 GeV/c^2) and $\sin^2\theta_W$ was taken to be 0.23. The branching ratios for τ decay were taken from [11], and the quark pair fragmentation into hadrons was modelled using the LUND Monte Carlo program JETSET7.2. The Monte Carlo events were passed through the detector simulation[12], and then through the same analysis program as the real data to determine the efficiencies of the selection criteria. Figure 2 also shows all the relevant distributions of the simulated events for M_χ=15 GeV/c^2, $M_{\chi'}$=60 GeV/c^2 and $\eta\eta' = -1$ (dotted histograms). For both $\eta\eta' = +1$ and $\eta\eta' = -1$, the detection efficiencies were estimated by Monte Carlo simulation for various points on the $(M_\chi, M_{\chi'})$ plane. The region $M_{\chi'} - M_\chi \leq 3$ GeV/c^2 was not considered because of the limitations of the fragmentation model. The efficiency of every point on the $(M_\chi, M_{\chi'})$ plane was obtained using the interpolation of the Monte Carlo results. The trigger efficiency was estimated to be greater than 95% from studies of the trigger efficiencies for multihadronic events and lepton-pair events. A systematic error of 10% was folded into the detection efficiency to take into account the uncertainties in the luminosity measurement, the detector simulation and the fragmentation model.

The upper limit (at the 95% confidence level) on the product of the branching ratios $BR(Z^0 \rightarrow \chi\chi' \rightarrow \chi\chi f\bar{f})$ was calculated from the number of the multihadronic events in the data sample used in this analysis (55150 events), the Z^0 total width (Γ_Z), the partial width into hadrons (Γ_{had}) and the detection efficiencies estimated above. For Γ_Z and Γ_{had} we have used again the values given in [10] (2.54 GeV and 1.84 GeV, respectively). Multihadronic events were selected according to [10]. The limits for $\eta\eta' = +1$ and $\eta\eta' = -1$ were calculated independently. The difference of these two limits is small, and at each point on the M_χ versus $M_{\chi'}$ plane we used the larger value to place the upper limit on the branching ratio. The limit on the branching ratio is shown in Figure 3 as a function of the neutralino masses.

The $\chi\chi' \rightarrow \chi\chi\gamma$ mode

Since the lightest neutralino χ is invisible, events from this process would be observed as "single photon" events. In order to select such events, the following selection cuts were applied.

(1) The energy deposited in the forward calorimeter had to be less than 5 GeV.

(2) There had to be no good track in the central detector.

(3) The event was vetoed if it contained more than one electromagnetic cluster consisting of more than one lead glass block and with a total cluster energy exceeding 2 GeV.

These cuts select events with a single neutral cluster. To select events well-contained in the barrel region and to reduce cosmic-ray backgrounds, the cluster was required to satisfy the following conditions:

(4) The corrected energy of the cluster had to be greater than 10 GeV. This energy correction was performed assuming the incident particle to be a photon. The distribution of the corrected energy is shown in Figure 4(a).

(5) The number of lead glass blocks of the cluster had to be greater than two, but less than or equal to 20.

(6) $|\cos\theta_\gamma| \leq 0.7$ where θ_γ is the angle between the cluster and the beam direction. Figure 4(b) shows the polar angular distribution of the neutral cluster.

To reject cosmic-ray backgrounds, the following selection criteria were required.

(7) There had to be no muon track in either the hadron calorimeter or in the muon chambers.

(8) The total energy deposit in the hadron calorimeter was required to be less than 8 GeV. The number of total hits of the hadron calorimeter strips in the layers from 3 to 9 had to be less than 2.

Some cosmic-ray backgrounds survived these cuts. Since the cluster shape from cosmic-rays was quite different from that of photons, a shower shape fit was performed on all remaining events. We defined the shower shape parameter $\chi^2_{\rm SF}$ as

$$\chi^2_{\rm SF} = \frac{1}{N_{\rm blk}-2}\sum_{i=1}^{N_{\rm blk}} \frac{(E_i^{\rm meas} - E_i^{\rm exp}(\theta,\phi))^2}{\sigma_i^2},$$

where $N_{\rm blk}$ is the number of blocks in the cluster, $E_i^{\rm meas}$ and $E_i^{\rm exp}$ are the measured and expected energies in the i-th block, and σ_i is the error on the measured energy. The incident angles of the photon (θ,ϕ) were iteratively determined to minimize the summation. The expected energy was calculated by numerical integration of the three dimensional shower profile function[13]. The $\chi^2_{\rm SF}$ distribution is shown in Figure 4(c). The distribution of $\chi^2_{\rm SF}$ of $e^+e^- \to \gamma\gamma$ events is also shown by the dotted line; a similar $\chi^2_{\rm SF}$ distribution is expected for 10 GeV $\leq E_\gamma \leq$ 46 GeV. The following cut was therefore applied to the remaining events:

(9) $\chi^2_{SF} \leq 4.0$.

The 8 events surviving this cut were visually scanned. Seven of these had one charged track far away from the beam interaction point associated to the electromagnetic cluster, and were identified as cosmic-ray backgrounds. One event had no charged track in the central detector and was identified as a single photon event. The energy of the photon in this event was 11 GeV.

The background from $e^+e^- \to \nu\bar{\nu}\gamma$ was calculated using the cross section as described in [14]. The expected number of events including detection efficiency for $E_\gamma \geq 10$ GeV and $|\cos\theta_\gamma| \leq 0.7$ is 0.6, consistent with the single observed event. In the calculation of limits, this event was treated as a possible signal.

The detection efficiency was estimated by Monte Carlo study. Final state particles $\chi\chi\gamma$ were generated by the matrix element[2];

$$\begin{aligned} &d\sigma(e^+(p_1)e^-(p_2) \to \chi(k_1)\chi'(q_2) \to \chi(k_1)\chi(k_2)\gamma(p_3)) \\ &\quad \propto (p_1\cdot k_1 p_2\cdot q_2 + p_1\cdot q_2 p_2\cdot k_1 - \eta\eta' p_1\cdot p_2 M_\chi M_{\chi'})d\Phi^{(3)}, \end{aligned}$$

where $p_1, p_2, q_2, k_1, k_2, p_3$ are 4-momenta and $d\Phi^{(3)}$ is the three-body phase space. η and η' are again the signs in the Majorana condition of χ and χ'. The energy and the polar angle of the photon were smeared according to the characteristics of the lead-glass calorimeter. The distributions of the photon energy and the polar angle of the Monte Carlo events ($M_\chi = 15$ GeV/c^2, $M_{\chi'} = 60$ GeV/c^2 and $\eta\eta' = -1$) are shown in Figure 4(a) and (b) by dotted lines. The inefficiency due to photon conversion in the inner part of the detector was estimated to be 16% from $e^+e^- \to \gamma\gamma$ events. Using the $e^+e^- \to e^+e^-$ events, the selection efficiencies of the cuts (5), (8) and (9) were estimated to

be 0.98, 0.91 and 0.98, respectively. The effects of initial state radiation reduce the acceptance by 4%. Since the energy deposited in the barrel electromagnetic calorimeter is expected to be greater than 8 GeV for the selected events, the trigger efficiency was estimated to be larger than 99.9%.

The systematic error in efficiency was taken to be 5%, including the uncertainties on the luminosity measurement and the Monte Carlo study. Contour plots of the upper limit of the branching ratio $BR(Z^0 \to \chi\chi' \to \chi\chi\gamma$ are shown in Figure 5. Again we took the larger value of the two limits on the branching ratio for $\eta\eta' = +1$ and $\eta\eta' = -1$.

Conclusions

Since the analyses of the decay modes $\chi' \to \chi f\bar{f}$ and $\chi' \to \chi\gamma$ are independent, we have combined these results to obtain an upper limit on the branching ratio $BR(Z^0 \to \chi\chi')$. Figure 6 shows the contour of the upper limit on $BR(Z^0 \to \chi\chi')$ as a function of M_χ and $M_{\chi'}$. In order to quote limits that are independent of the χ' branching ratio and the sign of $\eta\eta'$, at each point on the $(M_\chi, M_{\chi'})$ plane we have chosen the values of these parameters to give the maximum (worst-case) limit.

The partial width of $Z^0 \to \chi\chi'$ is given by [15]

$$\Gamma_{\chi\chi'} = \frac{G_F M_Z^3}{6\sqrt{2}\pi} A^2 \left[1 - \frac{(\eta m_\chi + \eta' m_{\chi'})^2}{s} + \frac{1}{2}\frac{(\eta m_\chi - \eta' m_{\chi'})^2}{s} - \frac{1}{2}\left(\frac{m_\chi^2 - m_{\chi'}^2}{s}\right)^2\right] \times \sqrt{1 - 2\frac{m_\chi^2 + m_{\chi'}^2}{s} + \left(\frac{m_\chi^2 - m_{\chi'}^2}{s}\right)^2}.$$

The effect of initial state radiation was included as described in [16]. Figure 7 shows the 95% C.L. upper limit on the mixing factor $|A|$ for each of the two cases $\eta\eta' = \pm 1$.

We have found no evidence for the events of $e^+e^- \to \chi\chi' \to \chi\chi f\bar{f}$ and $e^+e^- \to \chi\chi' \to \chi\chi\gamma$. Upper limits of a few 10^{-4} on the branching ratio of $BR(Z^0 \to \chi\chi')$ were obtained model independently for the range of neutralino masses accessible at LEP energies. Upper limits are also placed on the mixing factor of the neutralinos as a function of M_χ and $M_{\chi'}$. Similar or related studies have been presented by the MARK II[17], ALEPH[18], and DELPHI[19] collaborations.

Acknowledgement

It is a pleasure to thank the SL Division for the efficient operation of the LEP accelerator, the precise information on the absolute energy, and their continuing close cooperation with our experimental group. In addition to the support staff at our own institutions we are pleased to acknowledge the following :
Department of Energy, USA
National Science Foundation, USA
Science and Engineering Research Council, UK and The A.P. Sloan Foundation.
National Sciences and Engineering Research Council,Canada
Israeli Ministry of Science
Minerva Gesellschaft
The Japanese Ministry of Education, Science and Culture (the Monbusho) and a grant under the

Monbusho International Science Research Program.
American Israeli Bi-national Science Foundation.
L'Institut de Recherche Fondamentale du Commissariat à l'Energie Atomique, France.
The Bundesministerium für Forschung und Technologie, FRG.

References

[1] H. Haber and G. Kane, Phys. Rep. C117 (1985) 75 and references are therein.

[2] R. Barbieri et. al., Z Physics at LEP1, CERN 89-08 (1989) Vol. 2, 121.

[3] J. M. Frere and G. L. Kane, Nucl. Phys. B223 (1983) 331;
J. Ellis, J. S. Hagelin, D. V. Nanopoulos and M. Srednicki, Phys. Lett. 127B (1983) 233;
G. Gamberini, Z. Phys., C30 (1986) 605.

[4] J. Ellis, J. M. Frere, J. S. Hagelin, G. L. Kane and S. T. Petcov, Phys. Lett. 132B (1983) 436.

[5] H. Nilles, Phys. Rep. C10 (1984) 1;
R. Barbieri, Riv. Neuvo Cimento 11 (1988).

[6] OPAL Technical Proposal (1983) CERN/LEPC/83-4.

[7] S. Jadach, B. F. L. Ward, Z. Was, R. G. S. Stuart and W. Hollik, KORALZ the Monte Carlo Program for τ and μ pair production processes at LEP/SLC, unpublished (1989).

[8] T. Sjöstrand, Comp. Phys. Comm. 39 (1986) 347.

[9] JADE collab., W. Bartel et al., Z. Phys. C33 (1986) 23

[10] OPAL collab., M. Akrawy et al., Phys. Lett. 240B (1990) 497.

[11] Particle Data Group, G. P. Yost et al., Phys. Lett. 204B (1988) 1.

[12] J. Allison et al., Comp. Phys. Comm. 47 (1987) 55;
R. Brun et al., GEANT3, Report DD/EE/84-1, CERN (1989).

[13] E. Longo and I. Sestilli, Nucl. Inst. Method 128 (1975) 283.

[14] G. Barbielli, B. Richter and J. L. Siegrist, Phys. Lett. 106B (1981) 414.

[15] R. Barbieri, G. Gamberini, G. F. Giudice and G. Ridolfi, Phys. Lett. 195B (1987) 500.

[16] D. Bardin et al. Z Physics at LEP1, CERN 89-08 (1989) Vol. 1, 89.

[17] MARK II collab., T. Barklow et al., Phys. Rev. Lett. 64 (1990) 2984.

[18] ALEPH collab., D. Decamp et al., CERN-EP/90-63.

[19] DELPHI collab., P. Abreu et al., CERN-EP/90-80.

Figure Captions

Figure 1. (a) Visible energy ($E_{\rm vis}$) distribution of the real data sample and the Monte Carlo events for the $e^+e^- \to \tau\tau$ process. (b) The $E_{\rm vis}$ distributions of real data and Monte Carlo events for the multihadronic process. Dots indicate the distribution of the data sample and the histograms indicate the distribution of the Monte Carlo events.

Figure 2. The distributions of (a)visible energy ($E_{\rm vis}$), (b)acoplanarity angle ($\theta_{\rm acop}$) and (c)sum of the transverse momenta in the event ($P_{\rm T,sum}$) before applying the corresponding cuts. Solid histograms show the distribution for the data, while dotted histograms show those for the $\chi\chi f\bar{f}$ Monte Carlo events (M_χ = 15 GeV/c^2, $M_{\chi'}$ = 60 GeV/c^2 and $\eta\eta' = -1$). Arrows indicate the selection cuts. The Monte Carlo distribution is not normalized.

Figure 3. The 95% confidence level upper limit on the branching ratio BR($Z^0 \to \chi\chi' \to \chi\chi f\bar{f}$) is given as functions of M_χ and $M_{\chi'}$. The larger (worst case) value of the two cases $\eta\eta' = \pm 1$ has been used. Lines A,B,C, and D indicate the contours of 1.5, 2.0, 3.0, and 5.0 $\times$ 10^{-4}. The cross-hatched area is not considered in the analysis reported here, since we do not believe the Lund fragmentation to be reliable when the mass difference $M_{\chi'} - M_\chi$ is small.

Figure 4. The distributions of data (solid histogram) of (a)corrected energy deposition ($E_{\rm CLS}$), (b)cosine of the polar angular ($\cos\theta_\gamma$) and (c)shower shape fitting parameter ($\chi^2_{\rm SF}$) of the single neutral clusters before applying the corresponding selection criteria. In figures (a) and (b), the dotted histograms show the distribution of the same quantities of the simulated events for M_χ = 15 GeV/c^2, $M_{\chi'}$ = 60 GeV/c^2 and $\eta\eta' = -1$. In figure (c), the distribution of the shower shape parameter of $e^+e^- \to \gamma\gamma$ events is shown by the dotted histogram. The corresponding cuts are displayed by arrows. The Monte Carlo distributions are not normalized.

Figure 5. The 95% confidence level upper limit on the branching ratio BR($Z^0 \to \chi\chi' \to \chi\chi\gamma$) is shown as functions of M_χ and $M_{\chi'}$. Lines A,B, and C indicate the contours of 1.5, 2.0, and 3.0 $\times$ 10^{-4}. The larger (worst case) value of the two cases $\eta\eta' = \pm 1$ has been used. The cross-hatched area is kinematically inaccessible to the analysis reported here, since the maximum photon energy in this region would be less than the 10 GeV cut.

Figure 6. Upper limit on the branching ratio BR($Z^0 \to \chi\chi'$) at 95% confidence level. Curves A,B,C, and D indicate the contours of 1.5, 2.0, 3.0, and 5.0 $\times$ 10^{-4}. This limit is valid for all branching ratios BR($\chi' \to \chi\gamma$) and $\eta\eta' = \pm 1$. The cross-hatched area is not considered or not accessible to the analysis reported here.

Figure 7. The 95% confidence level upper limit on the mixing factor $|A|$ for (a) $\eta\eta' = -1$ and (b) $\eta\eta' = +1$. Curves A,B,C,D, and E indicate the contours of 0.04, 0.05, 0.075, 0.1, and 0.2. The cross-hatched area is not considered or not accessible to the analysis presented here.

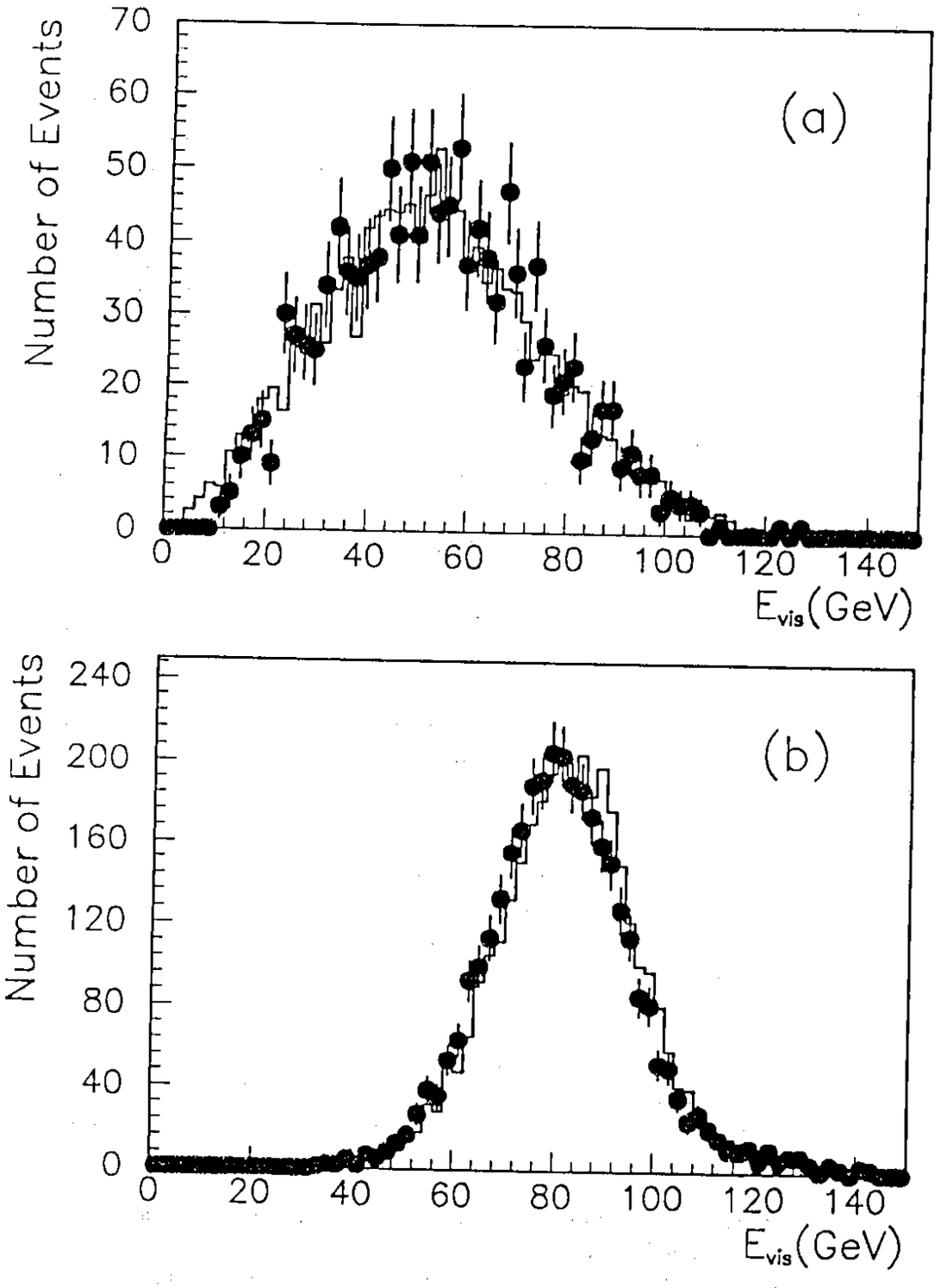
Number of Events
70
60
50
40
30
20
10
0
0
20
40
60
80
100
120
140
(a)
E_{vis}(GeV)
Number of Events
240
200
160
120
80
40
0
0
20
40
60
80
100
120
140
(b)
E_{vis}(GeV)

FIGURE.1

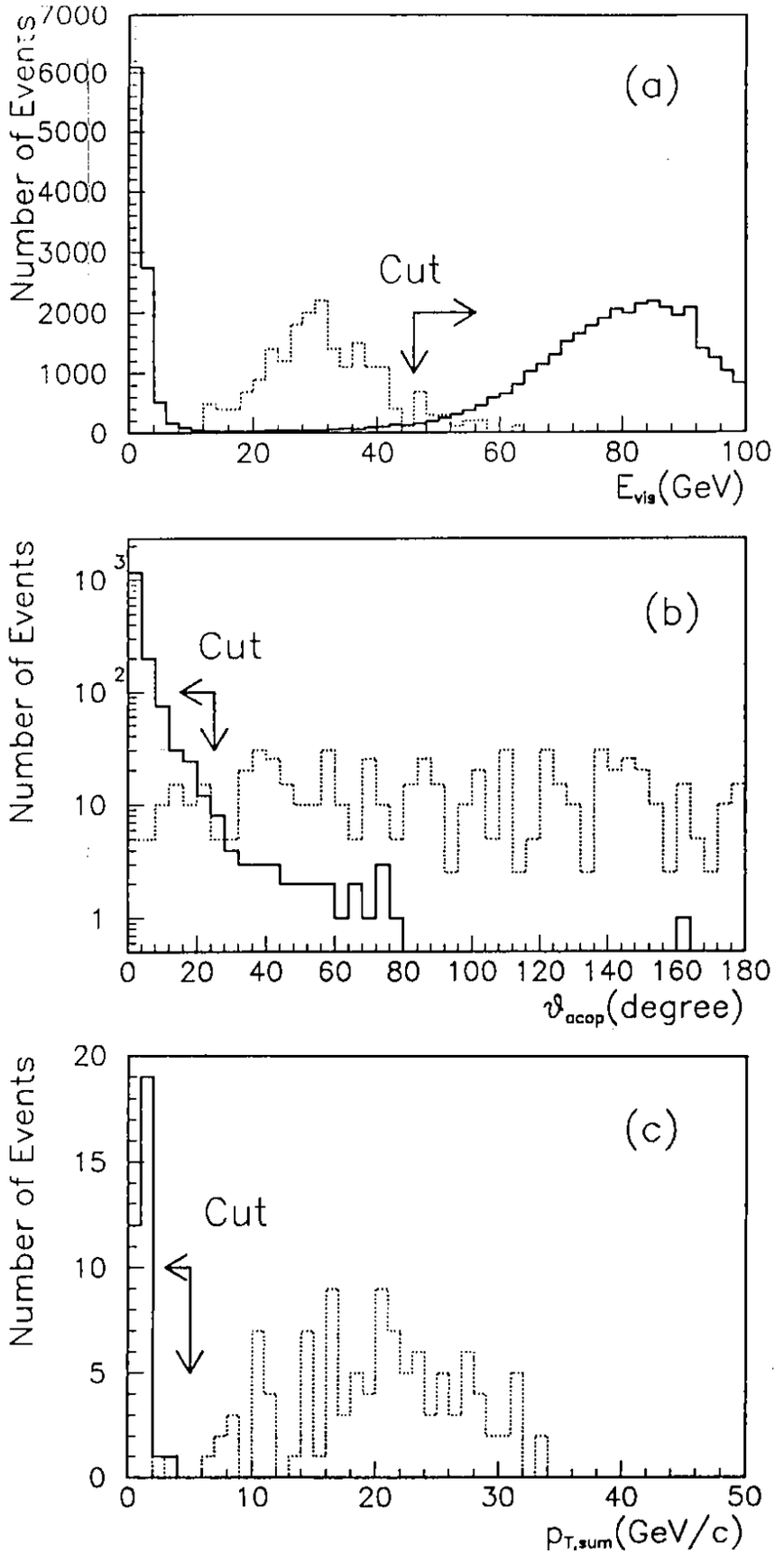
(a)
Cut
Number of Events
7000
6000
5000
4000
3000
2000
1000
0
0
20
40
60
80
100
E_{vis}(GeV)
(b)
Cut
Number of Events
10^3
10^2
10
1
0
20
40
60
80
100
120
140
160
180
ϑ_{acop}(degree)
(c)
Cut
Number of Events
20
15
10
5
0
0
10
20
30
40
50
$p_{T,sum}$(GeV/c)

FIGURE.2

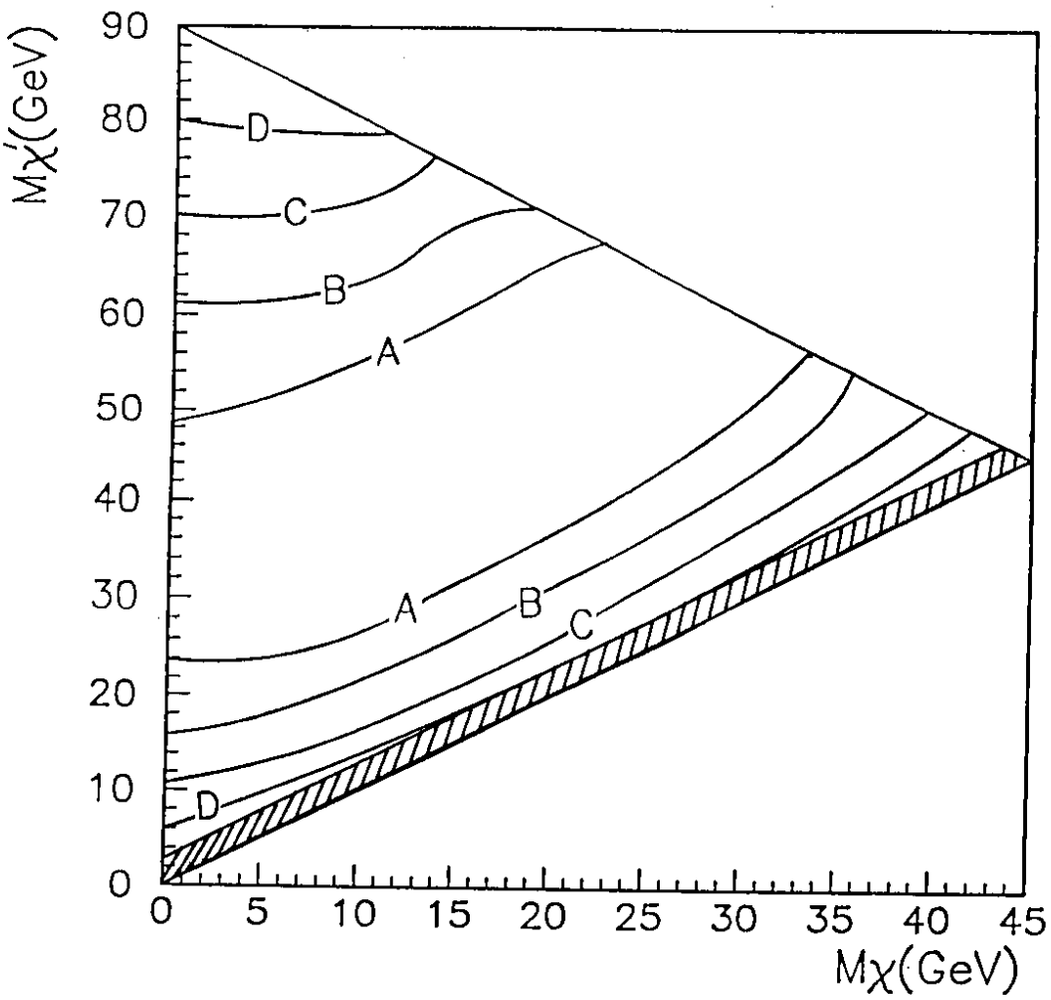
Mχ'(GeV)
90
80
70
60
50
40
30
20
10
0
D
C
B
A
A
B
C
D
0
5
10
15
20
25
30
35
40
45
Mχ(GeV)

FIGURE.3

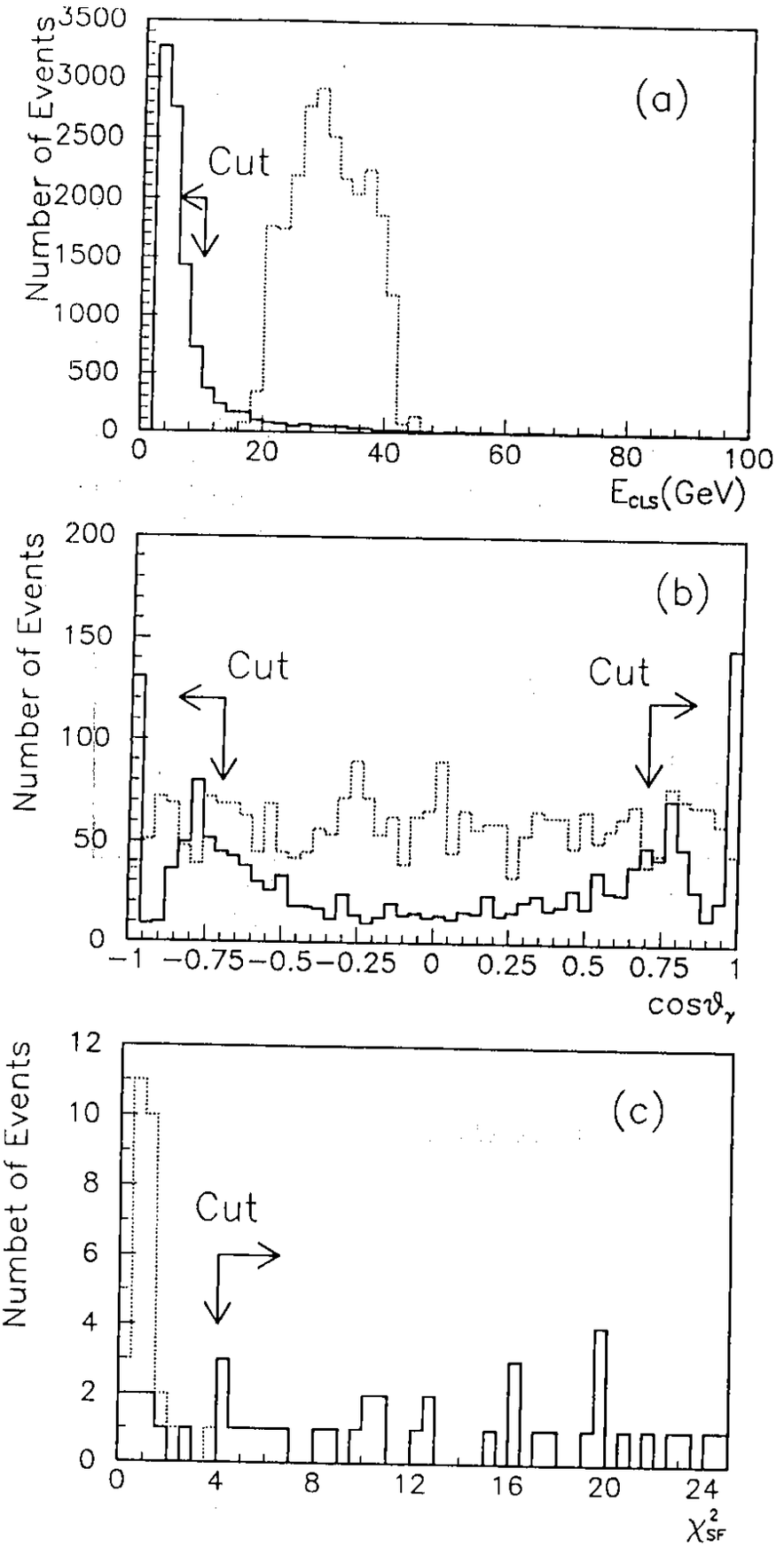
Number of Events
3500
3000
2500
2000
1500
1000
500
0
(a)
Cut
0
20
40
60
80
100
E_{CLS}(GeV)
Number of Events
200
150
100
50
0
(b)
Cut
Cut
−1
−0.75
−0.5
−0.25
0
0.25
0.5
0.75
1
$\cos\vartheta_\gamma$
Numbet of Events
12
10
8
6
4
2
0
(c)
Cut
0
4
8
12
16
20
24
χ^2_{SF}

FIGURE . 4

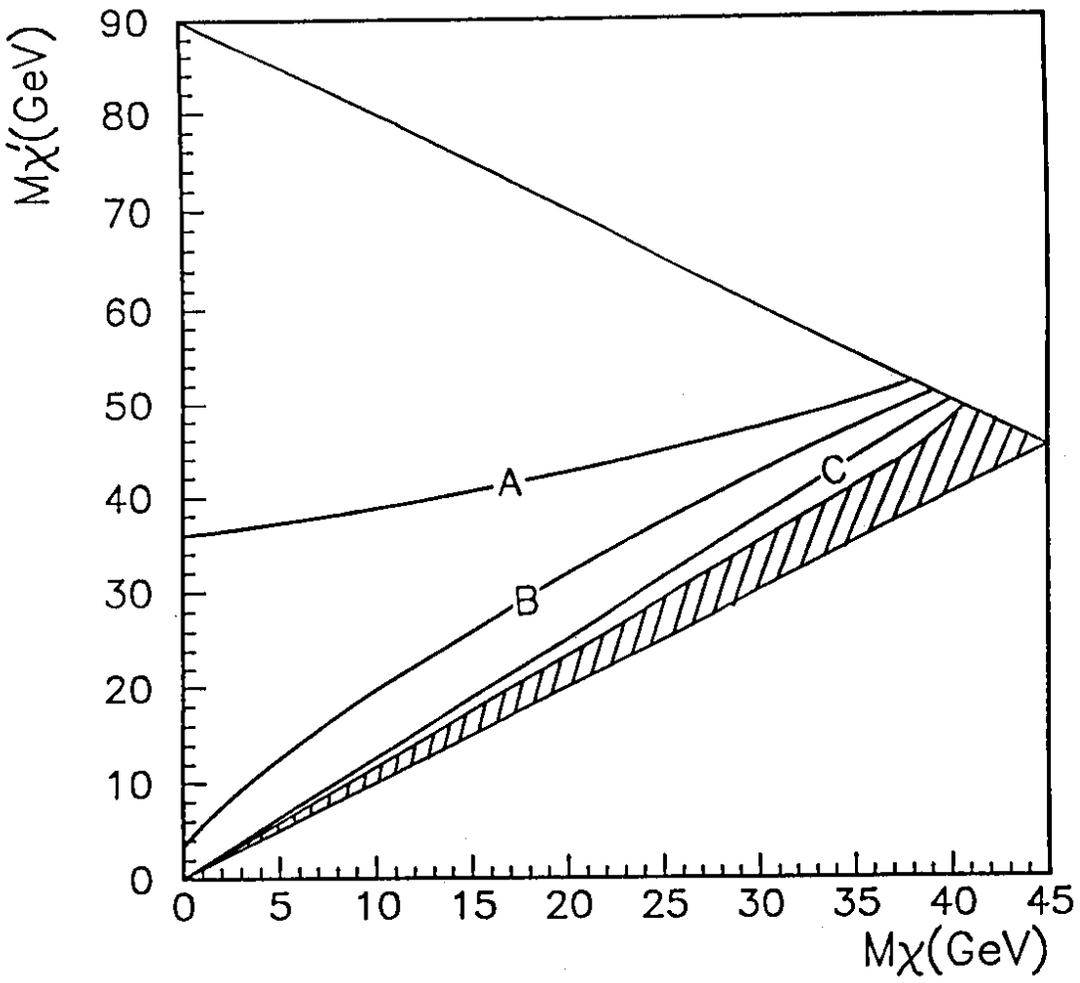
90
80
70
60
50
40
30
20
10
0
Mχ'(GeV)
A
B
C
0
5
10
15
20
25
30
35
40
45
Mχ(GeV)

FIGURE.5

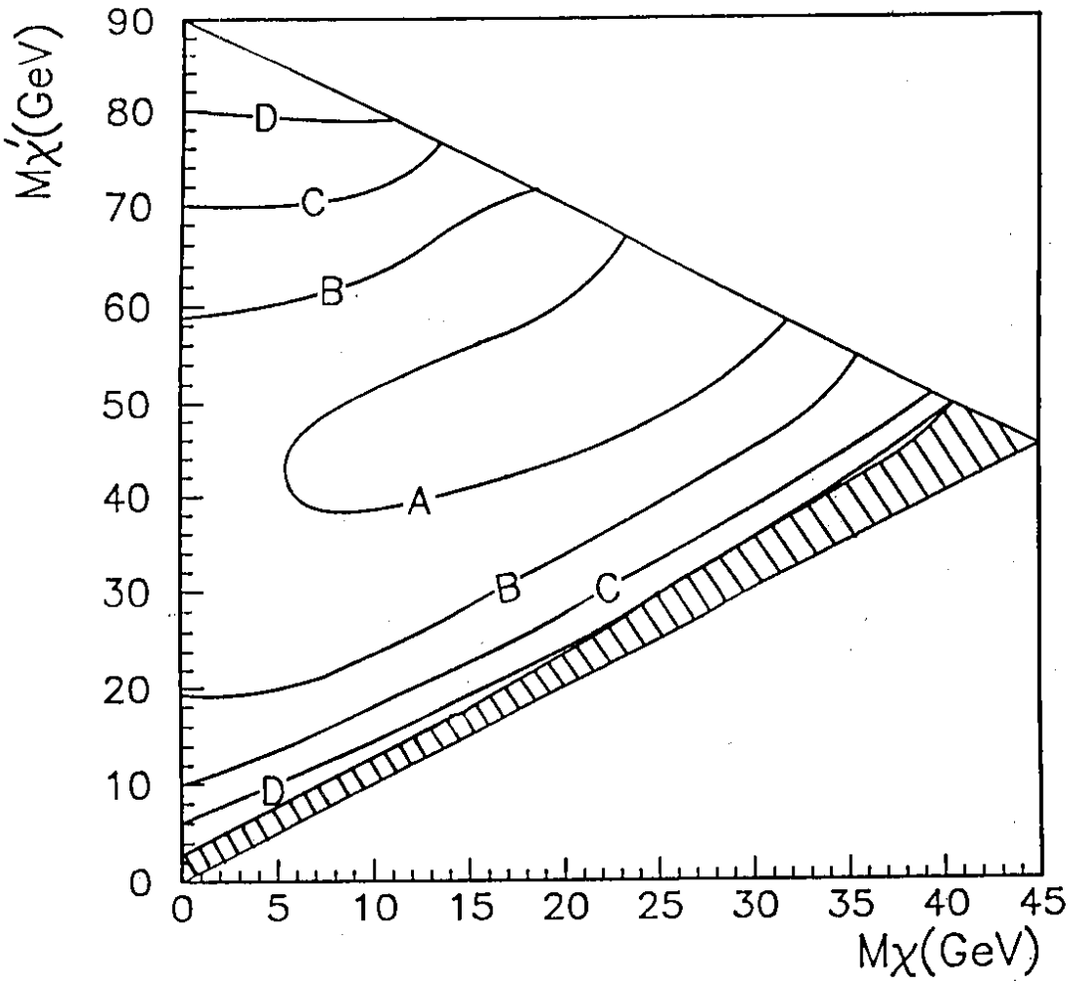
90
80
70
60
50
40
30
20
10
0
Mχ'(GeV)
D
C
B
A
B
C
D
0
5
10
15
20
25
30
35
40
45
Mχ(GeV)

FIGURE.6

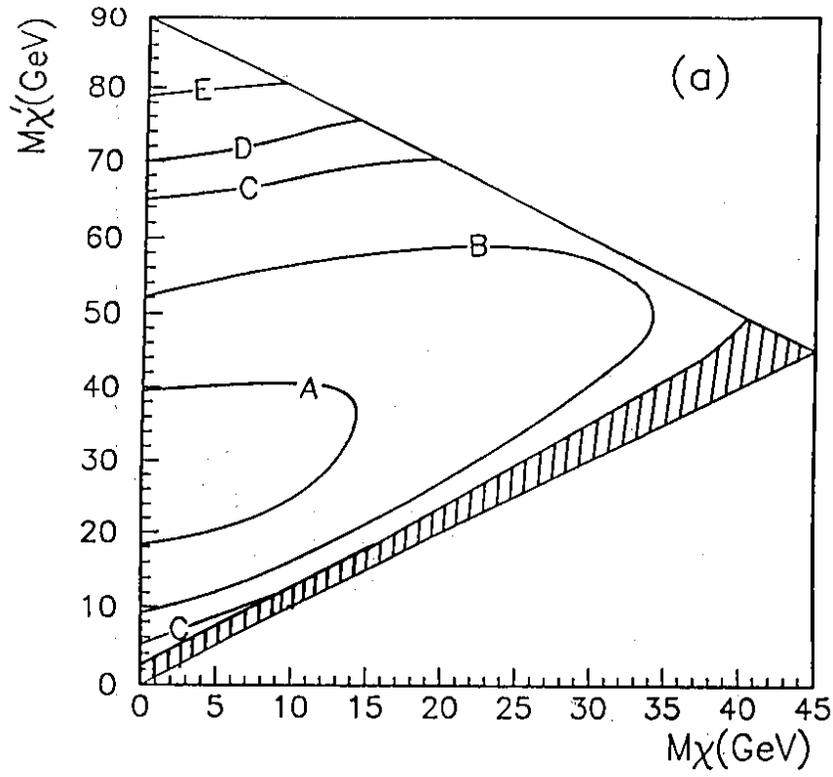

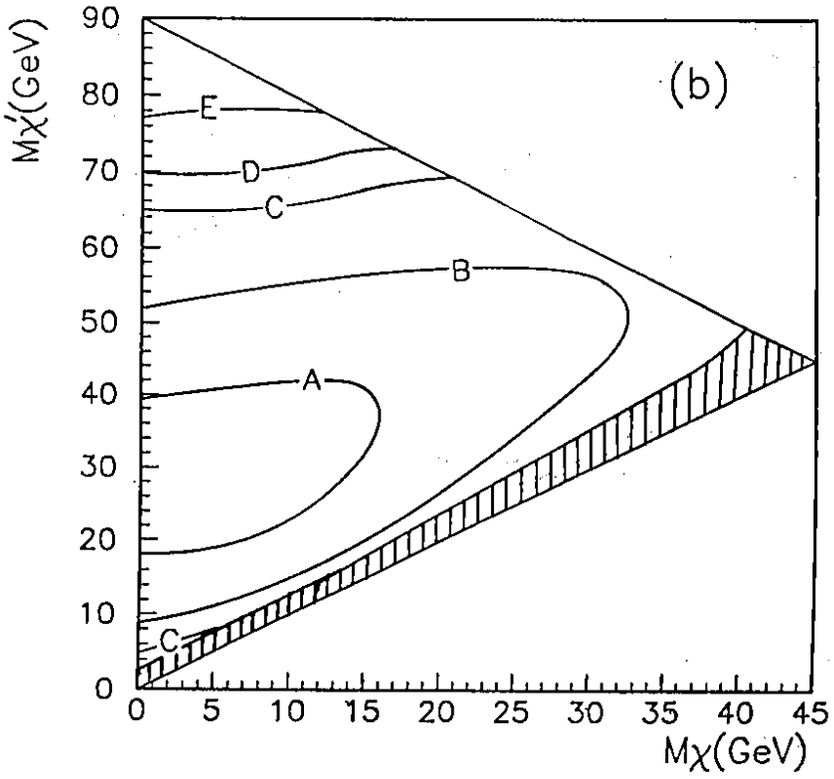

FIGURE.7

Imprimé au CERN. Prix : 0.60 Fr.